JACS
JOURNAL OF THE AMERICAN CHEMICAL SOCIETY

Communication

pubs.acs.org/JACS

Toward Understanding the Growth Mechanism: Tracing All Stable Intermediate Species from Reduction of Au(I)−Thiolate Complexes to Evolution of Au_{25} Nanoclusters

Zhentao Luo,[†] Vairavan Nachammai,[†] Bin Zhang,[†] Ning Yan,[†] David Tai Leong,[†] De-en Jiang,*[,‡,§] and Jianping Xie*[,†]

[†]Department of Chemical and Biomolecular Engineering, National University of Singapore, Singapore 119260

[‡]Chemical Sciences Division, Oak Ridge National Laboratory, Oak Ridge, Tennessee 37831, United States

Supporting Information

ABSTRACT: Despite 20 years of progress in synthesizing thiolated gold nanoclusters (Au NCs), the knowledge of their growth mechanism still lags behind. Herein the detailed process from reduction of Au(I)−thiolate complex precursors to the eventual evolution of and focusing to the atomically precise Au_{25} NCs was revealed for the first time by monitoring the time evolution of Au(I) precursor and Au NC intermediate species with ESI-MS. A two-stage, bottom-up formation and growth process was proposed: a fast stage of reduction-growth mechanism, followed by a slow stage of intercluster conversion and focusing. Balanced reactions of formation for each identified NC were suggested, backed by theoretical calculations of the thermodynamic driving force. This work advances one step further toward understanding the mechanism of formation and growth of thiolated Au NCs.

In the past two decades, sub-2 nm thiolate-protected gold nanoclusters (or thiolated Au NCs)[1] have attracted tremendous research interests because of their distinctive molecular-like properties such as quantized charging,[2] intrinsic chirality,[3] and photoluminescence.[4] Despite the great progress in synthesis and characterization, the mechanistic studies of NC formation still significantly lag behind.[5] The most common synthesis of thiolated Au NCs starts with the formation of polymeric Au(I)−thiolate complexes from the reaction between Au(III) salts and thiols, followed by reduction with excess borohydride. The resultant NCs can be converted into monodisperse or atomically precise NCs through a thermodynamic size selection (or size-focusing) process of thiol etching.[6] However, how the NCs are formed from the reduction of Au(I)−thiolate complexes, how they grow into a mixture of NCs, and how the magic sizes evolve out of the mixture are still experimentally unknown.

By employing a CO-directed, well-controlled reduction that transforms well-defined Au(I)−thiolate complexes into atomically precise thiolated Au_{25} NCs, here we identify all stable intermediate species using electrospray ionization mass spectrometry (ESI-MS)[7] and analyze their evolution throughout the course of synthesis. This time-tracing analysis reveals a bottom-up growth mechanism and novel reactive Au(I) complex precursors such as $[Au_3(SR)_3Cl]^-$ that are susceptible to CO reduction. The identified intermediates allow us to propose detailed, balanced chemical reactions for formation of every identified NC.

The facile one-pot CO-directed synthesis of thiolated Au_{25} NCs was based on a reported method.[8] We chose the mild gaseous reducing agent CO to ensure that the reduction kinetics is slow (relative to the reduction by borohydride) and can be readily stopped, so we could track the reaction intermediates. A simple thiol, 3-mercaptobenzoic acid (*m*-MBA), was used as the model thiolate ligand. In a typical synthesis, aqueous solutions of *m*-MBA (50 mM in 150 mM NaOH, 0.4 mL) and $HAuCl_4$ (40 mM, 0.25 mL) were added into a 25 mL round-bottom flask containing 9.5 mL ultrapure water under stirring (500 rpm). After 2 h, the color of the reaction solution turned light-yellow, indicating that Au(III) was reduced to Au(I) complexes. The pH of the solution was then brought to 11.6, and CO was bubbled through for 2 min. Then, the flask was sealed airtight, and the reaction was allowed to proceed for 72 h. Figure 1a illustrates the designed synthetic process, which starts with the kinetically controlled reduction of soluble Au(I)−thiolate complexes and the initial growth of NCs to form a mixture of thiolated Au NCs with a relatively narrow size distribution (Stage I); a long (~3 days) thermodynamically controlled size-focusing process then converts the mixed-sized NCs into thiolated Au_{25} NCs (Stage II).[6]

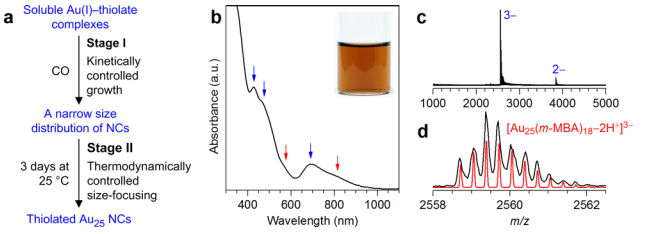

Figure 1. (a) Designed CO-directed synthesis of the atomically precise thiolated Au_{25} NCs. (b) UV−vis absorption and (c and d) ESI-MS spectra of the product obtained from the synthesis. Inset of (b), photo of the product under room light. The red line in (d) is the simulated isotope distribution of $[Au_{25}(m\text{-MBA})_{18} - 2H^+]^{3-}$.

Received: May 30, 2014
Published: July 11, 2014

   dx.doi.org/10.1021/ja505429f | J. Am. Chem. Soc. 2014, 136, 10577−10580

Before demonstrating the growth process, we first show that after Stage II highly pure $[Au_{25}(m\text{-MBA})_{18}]^-$ NCs were formed as the final product. The UV−vis absorption spectrum of the raw product shows well-defined features at 430, 480, and 690 nm (blue arrows in Figure 1b) and slight shoulder absorption peaks at ∼575 and ∼815 nm (red arrows in Figure 1b) which agrees well with the reported spectra of anionic thiolated Au_{25} NCs.[9] The yield of $[Au_{25}(m\text{-MBA})_{18}]^-$ was estimated to be >90% by comparing their molar absorptivity with Au_{25} NCs protected by glutathione (GSH).[7b] The ESI-MS spectrum of the product NCs (Figure 1c) displays only two sets of peaks at around 2580 (triply charged ions) and 3870 (doubly charged ions) m/z in the range of 1000−5000 m/z. Both sets of peaks are attributed to $[Au_{25}(m\text{-MBA})_{18}]^-$, corroborating the high purity of the NCs and the high yield of the synthesis. The isotope distribution of the base peak (Figure 1d, black line) matches with the simulated isotope distribution of $[Au_{25}(m\text{-MBA})_{18} - 2H^+]^{3-}$ (Figure 1d, red line), which confirms that the molecular formula of the final product is $[Au_{25}(m\text{-MBA})_{18}]^-$.

Now we show the reduction of Au(I)−thiolate complexes and the initial growth process of Au NCs. Both the UV−vis absorption (Figure 2a−c) and ESI-MS (Figure 2d,e) spectra of the reaction solution were measured at different time points starting from the moment immediately before the bubbling of CO (referred to as precursors) to 72 h after the bubbling of CO. The UV−vis absorption spectra of the reaction solution show a gradual increase in absorbance from 400 to 800 nm in the first 60 min (Figure 2a), indicating the formation and growth of thiolated Au NCs.[7b] Correspondingly, the color of the solution turned from light-yellow (color of the precursors) to yellow-brown to brown (insets of Figure 2a,b). From 60 min to 24 h, the UV−vis absorption spectra (Figure 2b) mainly show the growth of the characteristic peaks of $[Au_{25}(m\text{-MBA})_{18}]^-$ NCs, and these peaks become increasingly better defined from 24 to 72 h (Figure 2c). The color of the solution turned from brown to red-brown from 60 min to 72 h (Figure 2b,c insets).

ESI-MS spectra of the reaction solution (Figure 2d,e) were obtained with isotope resolution. Surprisingly, we were able to identify all the precursors and intermediates at different time points. The slow, mild, and readily stoppable CO reduction made this possible. In total, 29 species with a general molecular formula of $[Au_M(SR)_NCl_P]^q$ (where SR denotes *m*-MBA) were identified (see Figures S1−S29 for assignment). As shown in Figure 2e, right panel, these species can be classified into six groups according to the number of free valence electrons, $n^* = M - N - P - q$, where M, N, P, and q are the number of Au atoms, thiolate ligands, chloride ligands, and the net charge of the molecule, respectively.[10] All precursor species are Au(I) complexes ($n^* = 0$), confirming that the relatively low thiol-to-Au ratio used in our synthesis (2:1 as compared with the commonly used 3:1 or higher) is sufficient in reducing Au(III) to Au(I).[4c,11] The Au(I) complex precursors include the homoleptic Au(I)−thiolate complexes with the general formulas $Au_n(SR)_n$ and $[Au_n(SR)_{n+1}]^-$ and the heteroleptic Au(I) complexes that have both thiolate and chloride ligands $[Au_n(SR)_{n-p}Cl_{p+1}]^-$, where $p = 0$ or 1. The formation of $[Au_n(SR)_{n-p}Cl_{p+1}]^-$ is likely a result of the lack of free thiols due to the low thiol-to-Au ratio used in our synthesis because free thiols are able to replace the chloride ligands of Au(I)−chloride complexes in water or polar solvents.[12] The identified NCs all have even-numbered n^* ranging from 2 to 10. It is of

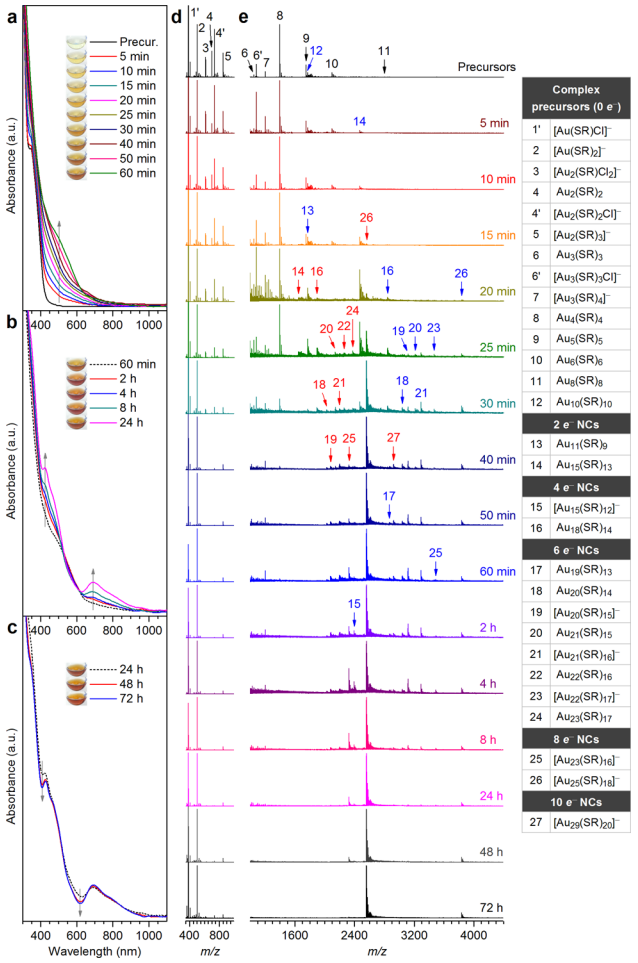

Figure 2. Time evolution of (a−c) UV−vis absorption and (d and e) ESI-MS spectra of the reaction solution during the synthesis of $[Au_{25}(SR)_{18}]^-$ (where SR denotes *m*-MBA). Insets in (a−c), photos of the reaction solution at different time points. The black, blue, and red labels in (d and e) indicate that the ionic species are singly, doubly, and triply charged, respectively. The right panel in (e) is the molecular formulas and the classification of the labeled species according to the number of free valence electrons (n^*).

note that many of the identified NCs here were reported previously, for example, by Negishi et al. via the separation of a mixture of GSH-protected Au NCs up to Au_{39} from $NaBH_4$ reduction.[7b] But the novelty of the present work is that we slowed down the reduction and traced the time evolution of the precursors and the intermediate NCs leading to highly pure $[Au_{25}(SR)_{18}]^-$, so we could better understand the formation and growth mechanism. To track each intermediate, we plot the time evolution of its ESI-MS peak intensity in Figure 3. At first sight, one can see two distinctive stages as suggested in Figure 1a. Stage I (the first ∼40 min) was the kinetically controlled growth of the NCs, which converted most Au(I) complexes into a narrow distribution of intermediate NCs with n^* ranging from 4 e^- to 10 e^-. Stage II (from ∼40 min onward) was the thermodynamically controlled, slow size-focusing process in which intermediate NCs converged to the thermodynamically stable $[Au_{25}(SR)_{18}]^-$.

Stage I was initiated by CO reduction of Au(I) complex precursors: $Au_n(SR)_n$, $[Au_n(SR)_{n+1}]^-$, and $[Au_n(SR)_{n-p}Cl_{p+1}]^-$. Figure S30 shows their DFT-optimized structures. $Au_n(SR)_n$ (when $n > 2$) complexes are cyclic,[13] whereas the

dx.doi.org/10.1021/ja505429f | J. Am. Chem. Soc. 2014, 136, 10577−10580

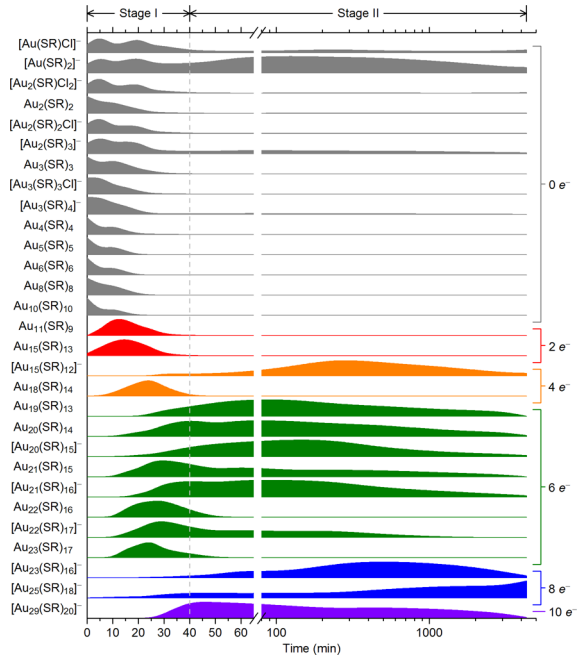

Figure 3. Normalized ESI-MS spectral intensity profiles of the complex and NC species throughout the synthesis.

$[Au_n(SR)_{n-p}Cl_{p+1}]^-$ complexes are linear and can be considered as $[Au_n(SR)_{n+1}]^-$ with one or both of the terminal thiolate ligands replaced by chloride. Figure 3 shows that $Au_n(SR)_n$ and $[Au_n(SR)_nCl]^-$ ($n > 1$) were consumed rapidly and completely during Stage I, whereas some $[Au_n(SR)_{n+1}]^-$ species ($n = 1$ and 2) remained in the reaction solution throughout Stage II despite excess CO (~70 equiv of Au), suggesting that these $[Au_n(SR)_{n+1}]^-$ species were much less reactive toward reduction by CO.

Consumption of reactive $Au_n(SR)_n$ and $[Au_n(SR)_nCl]^-$ species leads to formation of $Au_M(SR)_N$ ($M > N$) NCs. Figure 3 shows that 2 e^- NCs including $Au_{11}(SR)_9$ and $Au_{15}(SR)_{13}$ were formed first. To our knowledge, this is the first time that $Au_{11}(SR)_9$ has been observed. How does the reduction of $Au_n(SR)_n$ and $[Au_n(SR)_nCl]^-$ species lead to $Au_{11}(SR)_9$ or $Au_{15}(SR)_{13}$? We propose a reduction-growth mechanism for the 2 e^- NC formation, which consists of a reduction step and a subsequent growth step. We hypothesize that the reduction step happens via binding of CO to Au(I) of the reactive Au(I) complex precursors to form a linear monocarbonyl Au(I)–thiolate complex $Au_n(SR)_nCO$. The carbonyl group then reacts with the abundant hydroxide ions in the reaction solution (at pH 11.6) through a classic Hieber base reaction to form a metallacarboxylic acid $[Au_n(SR)_nCOOH]^-$.[14] The decarboxylation of this intermediate drives the transfer of two electrons to the nearby two Au(I) atoms to reduce them to Au(0) and form a Au–Au bond. The decarboxylation mechanism is supported by a total inorganic carbon analysis which indicates a stoichiometric amount of CO_3^{2-} is present in the final reaction solution (see SI). After losing two $^-$SR groups, a charge-neutral 2 e^- NC intermediate $Au_n(SR)_{n-2}$ is formed.[15] See Figure S31 for the details of the proposed CO reduction mechanism. As no signals of carbonyl or carboxyl Au(I) complexes were observed in ESI-MS (Figure 2d,e) or FTIR (Figure S33) analyses, the binding of CO to Au(I) is likely rate-determining. The $Au_n(SR)_{n-2}$ from this step is small (n is from 2 to 10, limited by the precursor sizes) and expected to be very labile as their cores are quite open and susceptible to chemical attacks and further reactions.[16] In the growth step, these small $Au_n(SR)_{n-2}$ NC intermediates will collide with another complex precursor and coalesce into a larger and more stable NC. This proposed two-step reduction-growth formation of the 2 e^- NC $Au_{11}(SR)_9$ can be written as in Scheme 1: the $Au_6(SR)_6$ precursor is

Scheme 1. Proposed Reduction-Growth Formation of $Au_{11}(SR)_9$

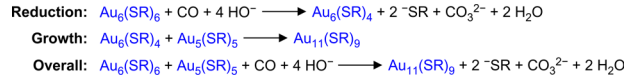

reduced by CO to $Au_6(SR)_4$ which subsequently reacts with the $Au_5(SR)_5$ precursor to form $Au_{11}(SR)_9$. Using density functional theory with a continuum solvation model, we computed the overall reaction enthalpy for $Au_{11}(SR)_9$ formation in water according to Scheme 1 and found it to be about −155 kcal/mol (see SI), indicating that the proposed reaction has a very favorable thermodynamic driving force. Likewise, $Au_{15}(SR)_{13}$ can be formed from the reduction-growth process that involves $Au_{10}(SR)_{10}$ and $Au_5(SR)_5$ and the computed reaction enthalpy is at −161 kcal/mol.

Figure 3 shows that the initial formation of 4, 6, 8, and 10 e^- NCs also occurred in Stage I, slightly after 2 e^- NCs. The temporal ordering of appearance suggests a sequential 2 e^- reduction-growth process: 2 e^- → 4 e^- → 6 e^- → 8 e^- → 10 e^- (Figure S32). For example, the 4 e^- $Au_{18}(SR)_{14}$ can be formed from CO reduction of $Au_3(SR)_3$ to $Au_3(SR)_1$ followed by its reaction with 2 e^- $Au_{15}(SR)_{13}$. In other words, Figure 3 suggests a bottom-up formation process via reduction-growth from the reactive Au(I) precursors to thiolated Au NCs with sequentially larger and even n*. The clear end of Stage I (or the relatively fast bottom-up growth of NCs) is a result of the depletion of reactive Au(I)–thiolate complex precursors that fueled the growth of NCs.

Stage II is characterized by the relatively slow size-focusing process that eventually produced the highly pure $[Au_{25}(SR)_{18}]^-$. Conventional size-focusing method usually involves etching a mixture of larger NCs into smaller, more stable NCs and Au(I)–thiolate complexes by using excess thiols at elevated temperatures.[17] The size-focusing process here is different in that it involves mainly conversion of smaller NCs to larger ones. ESI-MS spectra suggest that there are at least three modes of NC interconversion and growth in Stage II: isoelectronic addition, disproportionation, and comproportionation reactions. For example, the ESI-MS spectra (Figures 2d,e and 3) and the residual UV–vis absorption spectra (Figure S34) indicate the growth of $[Au_{23}(SR)_{16}]^-$ into $[Au_{25}(SR)_{18}]^-$ from 24 to 72 h. The structures of $[Au_{23}(SR)_{16}]^-$ and $[Au_{25}(SR)_{18}]^-$ are highly symmetrical and closely related[18] and differ in their molecular formulas by a $Au_2(SR)_2$. While $Au_2(SR)_2$ or $[Au_2(SR)_2Cl]^-$ was in negligible amounts, $[Au(SR)Cl]^-$ was abundant in the reaction solution in the period of 24–72 h (Figure 2d). Thus, $[Au_{23}(SR)_{16}]^-$ may slowly grow into $[Au_{25}(SR)_{18}]^-$ by isoelectronic addition of two units of –Au(SR)– as in Reaction **1**, Scheme 2. Enthalpy for this reaction computed from DFT is −11 kcal/mol, confirming that conversion of $[Au_{23}(SR)_{16}]^-$ to $[Au_{25}(SR)_{18}]^-$ is indeed thermodynamically favorable, though this driving force is much smaller than those of the reduction-growth reactions in Stage I, consistent with the slow pace of Stage II conversions.

dx.doi.org/10.1021/ja505429f | J. Am. Chem. Soc. 2014, 136, 10577–10580

Scheme 2. Isoelectronic Addition, Disproportionation, and Comproportionation Reactions Occurred during the Size-Focusing Process (Stage II) of the Synthesis

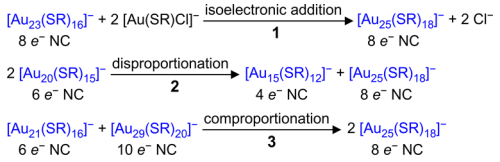

Formation of 4 e^- $[Au_{15}(SR)_{12}]^-$ well after 6 e^-, 8 e^-, and 10 e^- NCs in Stage II (Figure 3) suggests a disproportionation reaction, for example, between two $[Au_{20}(SR)_{15}]^-$ as shown by Reaction **2**, Scheme 2.[19] Consumption of $[Au_{29}(SR)_{20}]^-$ (10 e^-) indicates a reaction with another NC such as $[Au_{21}(SR)_{16}]^-$ to produce two $[Au_{25}(SR)_{18}]^-$ via a comproportionantion reaction (Reaction **3**, Scheme 2). Besides these three modes of reactions, the reduction by CO still occurs to increase n^* of some intermediate NCs, but the reduction rate is much slower than that of Stage I due to the lack of reactive complexes or complex motifs on the NC surface.[20] On the basis of the observed time evolution of the NC species (Figures 2 and 3) and the above analyses of Stages I and II, we proposed plausible chemical equations of the formation and consumption of all the observed NCs during the synthesis (see SI), which can serve as hypotheses for future studies of the growth mechanism.

In conclusion, we have monitored the entire transformation from Au(I) complex precursors to $[Au_{25}(SR)_{18}]^-$ using UV−vis spectroscopy and ESI-MS, enabled by the mild CO reduction. Au(I)−thiolate complex precursors (including chloride-containing ones) and stable NC intermediates have been clearly identified. On the basis of the time evolution of those species, we were able to propose a reduction-growth mechanism of the kinetically controlled NC formation in the fast Stage I and intercluster conversion pathways in the subsequent, thermodynamically controlled size-focusing to $[Au_{25}(SR)_{18}]^-$ (Stage II). The present results represent an important step forward toward understating the growth mechanism of thiolated Au NCs and call for further time-resolved studies of precursor reduction and NC growth and interconversion, in an effort to shed light on synthetic processes and to facilitate the development of synthetic strategies for new NCs.

■ ASSOCIATED CONTENT

Supporting Information

Experimental and computational details, characterization data, and proposed reactions and mechanisms. This material is available free of charge via the Internet at http://pubs.acs.org.

■ AUTHOR INFORMATION

Corresponding Author

*chexiej@nus.edu.sg; djiang@ucr.edu

Present Address

[§]Department of Chemistry, University of California, Riverside, California 92521, United States.

Notes

The authors declare no competing financial interest.

■ ACKNOWLEDGMENTS

This work is financially supported by the Ministry of Education, Singapore, under Grant R-279-000-409-112. DFT computation was supported by the Division of Chemical Sciences, Geosciences, and Biosciences, Office of Basic Energy Sciences, U.S. Department of Energy.

■ REFERENCES

(1) (a) Kim, B. H.; Hackett, M. J.; Park, J.; Hyeon, T. *Chem. Mater.* **2013**, *26*, 59. (b) Jin, R. *Nanoscale* **2010**, *2*, 343. (c) Lu, Y.; Chen, W. *Chem. Soc. Rev.* **2012**, *41*, 3594. (d) Tsukuda, T. *Bull. Chem. Soc. Jpn.* **2012**, *85*, 151. (e) Negishi, Y.; Kurashige, W.; Niihori, Y.; Nobusada, K. *Phys. Chem. Chem. Phys.* **2013**, *15*, 18736.

(2) (a) Laaksonen, T.; Ruiz, V.; Liljeroth, P.; Quinn, B. M. *Chem. Soc. Rev.* **2008**, *37*, 1836. (b) Murray, R. W. *Chem. Rev.* **2008**, *108*, 2688.

(3) (a) Jadzinsky, P. D.; Calero, G.; Ackerson, C. J.; Bushnell, D. A.; Kornberg, R. D. *Science* **2007**, *318*, 430. (b) Hakkinen, H. *Nat. Chem.* **2012**, *4*, 443. (c) Dolamic, I.; Knoppe, S.; Dass, A.; Bürgi, T. *Nat. Commun.* **2012**, *3*, 798.

(4) (a) Shang, L.; Dong, S.; Nienhaus, G. U. *Nano Today* **2011**, *6*, 401. (b) Zheng, J.; Zhou, C.; Yu, M.; Liu, J. *Nanoscale* **2012**, *4*, 4073. (c) Luo, Z.; Yuan, X.; Yu, Y.; Zhang, Q.; Leong, D. T.; Lee, J. Y.; Xie, J. *J. Am. Chem. Soc.* **2012**, *134*, 16662. (d) Yu, Y.; Luo, Z.; Chevrier, D. M.; Leong, D. T.; Zhang, P.; Jiang, D.-e.; Xie, J. *J. Am. Chem. Soc.* **2014**, *136*, 1246.

(5) Liu, C.; Li, G.; Pang, G.; Jin, R. *RSC Adv.* **2013**, *3*, 9778.

(6) (a) Wu, Z.; Suhan, J.; Jin, R. *J. Mater. Chem.* **2009**, *19*, 622. (b) Dharmaratne, A. C.; Krick, T.; Dass, A. *J. Am. Chem. Soc.* **2009**, *131*, 13604. (c) Jin, R.; Qian, H.; Wu, Z.; Zhu, Y.; Zhu, M.; Mohanty, A.; Garg, N. *J. Phys. Chem. Lett.* **2010**, *1*, 2903.

(7) (a) Schaaff, T. G.; Knight, G.; Shafigullin, M. N.; Borkman, R. F.; Whetten, R. L. *J. Phys. Chem. B* **1998**, *102*, 10643. (b) Negishi, Y.; Nobusada, K.; Tsukuda, T. *J. Am. Chem. Soc.* **2005**, *127*, 5261.

(8) (a) Yu, Y.; Luo, Z.; Yu, Y.; Lee, J. Y.; Xie, J. *ACS Nano* **2012**, *6*, 7920. (b) Yu, Y.; Chen, X.; Yao, Q.; Yu, Y.; Yan, N.; Xie, J. *Chem. Mater.* **2013**, *25*, 946.

(9) Zhu, M.; Eckenhoff, W. T.; Pintauer, T.; Jin, R. *J. Phys. Chem. C* **2008**, *112*, 14221.

(10) Pei, Y.; Zeng, X. C. *Nanoscale* **2012**, *4*, 4054.

(11) Shaw, C. F.; Cancro, M. P.; Witkiewicz, P. L.; Eldridge, J. E. *Inorg. Chem.* **1980**, *19*, 3198.

(12) (a) Goulet, P. J. G.; Lennox, R. B. *J. Am. Chem. Soc.* **2010**, *132*, 9582. (b) Li, Y.; Zaluzhna, O.; Xu, B.; Gao, Y.; Modest, J. M.; Tong, Y. J. *J. Am. Chem. Soc.* **2011**, *133*, 2092.

(13) Grönbeck, H.; Walter, M.; Häkkinen, H. *J. Am. Chem. Soc.* **2006**, *128*, 10268.

(14) Steinborn, D. *Fundamentals of Organometallic Catalysis*, 1st ed.; Wiley-VCH: Weinheim, Germany, 2012.

(15) Guidez, E. B.; Hadley, A.; Aikens, C. M. *J. Phys. Chem. C* **2011**, *115*, 6305.

(16) Jiang, D.-e.; Whetten, R. L.; Luo, W.; Dai, S. *J. Phys. Chem. C* **2009**, *113*, 17291.

(17) (a) Shichibu, Y.; Negishi, Y.; Tsunoyama, H.; Kanehara, M.; Teranishi, T.; Tsukuda, T. *Small* **2007**, *3*, 835. (b) Qian, H.; Zhu, Y.; Jin, R. *ACS Nano* **2009**, *3*, 3795. (c) Nimmala, P. R.; Jupally, V. R.; Dass, A. *Langmuir* **2014**, *30*, 2490.

(18) (a) Zhu, M.; Aikens, C. M.; Hollander, F. J.; Schatz, G. C.; Jin, R. *J. Am. Chem. Soc.* **2008**, *130*, 5883. (b) Heaven, M. W.; Dass, A.; White, P. S.; Holt, K. M.; Murray, R. W. *J. Am. Chem. Soc.* **2008**, *130*, 3754. (c) Das, A.; Li, T.; Nobusada, K.; Zeng, C.; Rosi, N. L.; Jin, R. *J. Am. Chem. Soc.* **2013**, *135*, 18264.

(19) Zeng, C.; Liu, C.; Pei, Y.; Jin, R. *ACS Nano* **2013**, *7*, 6138.

(20) (a) Pei, Y.; Pal, R.; Liu, C.; Gao, Y.; Zhang, Z.; Zeng, X. C. *J. Am. Chem. Soc.* **2012**, *134*, 3015. (b) Jiang, D.-e.; Chen, W.; Whetten, R. L.; Chen, Z. *J. Phys. Chem. C* **2009**, *113*, 16983.